Kinetics of liquid-solid phase transition in large nickel clusters

Alexander V. Yakubovich,* Gennady Sushko, Stefan Schramm, and Andrey V. Solov'yov
Frankfurt Institute for Advanced Studies, Ruth-Moufang-Str. 1, 60438 Frankfurt am Main, Germany
(Received 12 October 2012; published 23 July 2013)

In this paper, we have explored computationally the solidification process of a nickel cluster consisting of 2057 atoms. This process has the characteristic features of the first-order phase transition occurring in a finite system. The focus of our research is placed on the elucidation of correlated dynamics of a large ensemble of particles in the course of the nanoscale liquid-solid phase transition through the computation and analysis of the results of molecular dynamics (MD) simulations with the corresponding theoretical model. This problem is of significant interest and importance because the controlled dynamics of systems on the nanoscale is one of the central topics in the development of modern nanotechnologies. MD simulations in large molecular systems are rather computer power demanding. Therefore, in order to advance with MD simulations, we have used modern computational methods based on the graphics processing units (GPUs). The advantages of the use of GPUs for MD simulations in comparison with the CPUs are demonstrated and benchmarked. The reported speedup reaches factors greater than 400. This work opens a path towards exploration with the use of MD of a larger number of scientific problems inaccessible earlier with the CPU-based computational technology.

DOI: 10.1103/PhysRevB.88.035438 PACS number(s): 36.40.Ei, 02.70.−c, 64.60.an

I. INTRODUCTION

The melting process in a macroscopically large system occurs at a certain temperature under fixed external pressure. This process is a first-order phase transition and it manifests itself as a spike in the heat capacity of the system at the transition temperature. In crystals, the reverse process of freezing or solidification is often observed at a temperature significantly below the thermodynamic melting point due to the nucleation nature of the solidification phase transitions.[1]

In small systems, the finite volume that is available for the precursor formation alters the kinetics of the solidification phase transition. The study of supercooled metal droplets of the size of several micrometers was performed in the early 1950s.[2,3] In Ref. 3, it was shown that the mercury droplets of 2–8 μm in diameter solidify at rates that are proportional to the droplet volume. In systems of nanometer size, the ratio of the surface to volume atoms increases and the reduced binding energy of the surface atoms changes significantly the total energy of the system. The first thermodynamic model bridging the melting point of the clusters with their size was proposed by Pawlow more than a century ago.[4] In multiple subsequent works it was confirmed that the melting temperature of a small spherical particle decreases with the reduction of its radius.[5–8] In small particles, the relative fraction of the surface atoms is higher, which leads to the decrease of the melting temperature. This size effect has been confirmed for the clusters having diameters down to 2 nm.[5] Its explanation is based on the characteristic radial dependence of the ratio of the surface to volume energy of a finite system.

However, for clusters having sizes smaller than 1–2 nm, the melting temperature is no longer a monotonic function of the cluster size. Experiments on sodium clusters Na_N with number of atoms $N = 50$–360 have demonstrated that the melting temperature as a function of size shows a prominent irregular structure with local maxima.[9–12] The origin of the nonmonotonic variation in the melting temperature with respect to cluster size lies in the interplay between electronic and geometric shell effects in the sodium clusters and the entropy change in the course of such nanoscale phase transitions.[12]

Intensive theoretical efforts have been undertaken to identify the details of the geometric and electronic structures underlying the variations in the melting temperature.[13–20] Experiments on small ion clusters of tin[21] and gallium[22] have confirmed the violation of the linear relationship between the reduction in the melting temperature and the inverse radius of the cluster. It was discovered that the melting temperature of selected Sn_N and Ga_N clusters, of sizes $N < 40$, can considerably exceed the melting temperature of the corresponding bulk material.[21,22] This behavior was explained by the structural differences between the small clusters and the bulk.[21]

There are also other factors which affect the melting temperatures of small clusters. For instance, impurities play a significant role. Thus, in Ref. 23 it was demonstrated that a single atom impurity leads to significant changes in the thermodynamic properties of the Ni_{147} cluster. Also, the melting temperatures differ significantly in nanoalloys as compared to pure materials. In Ref. 24 it was shown that alloying iron clusters consisting of up to 2400 atoms with carbon reduces their melting temperature by 100–150 K at a carbon concentration of 10%–12%. Recently, the thermal behavior of free and alumina-supported Fe-C nanoparticles has been investigated.[25] It was observed that the presence of the substrate raises the melting temperature of medium and large $Fe_{(1-x)N}C_{xN}$ nanoparticles ($x = 0$–0.16, $N = 80$–1000) by 40–60 K.[25] In Ref. 26, the freezing-melting hysteresis associated with a free-energy barrier between solid and liquid phases was investigated theoretically for the materials in pores.

There are many papers devoted to the computer simulations of the melting process of metal clusters consisting of up to few hundreds of atoms. For the small systems, one can utilize approaches based on density functional theory,[27] Car-Parinello molecular dynamics (MD),[28] or tight-binding schemes.[29] The aforementioned methods are capable of reproducing relatively accurately the structural and energetic properties

of the clusters. However, computational complexity of the aforementioned methods does not allow for modeling of metal clusters consisting of thousands of atoms on the time scales exceeding nanoseconds.

Investigations of melting of clusters of several thousands of atoms are carried out using empirical classical potentials for the description of interatomic interactions. The delocalized nature of *d* electrons in the transition-metal clusters implies utilization of so-called many-body potentials. The widely used potentials for the description of interactions between nickel atoms are based on the so-called embedded atom model, to which belong Sutton-Chen and Finnis-Sinclair potentials. In Ref. 30, MD simulations of melting and solidification of Ni nanoclusters with up to 8007 atoms are performed with the use of the classical quantum-corrected Sutton-Chen potential,[31] and the characteristics of the liquid-solid phase transition are analyzed for different cluster sizes. The investigation of melting and solidification of Ni clusters consisting of up to 32 000 atoms using the conventional Sutton-Chen potential is presented in Ref. 32. In that paper, the reduction of the melting and solidification temperatures for the face-centered-cubic (fcc) metals is reported to be negatively correlated with the particle radius, and the Gibbs-Thomson coefficient is found to be proportional to the melting point. In Ref. 33, the investigation of the effect of the cooling rate on the final structure of Mo_{6750} clusters is performed with the use of the Finnis-Sinclair potential.

In this paper, we conduct MD simulations of Ni_{2057} clusters on the time scale up to 65 ns and discuss the kinetics of the solidification phase transition for the clusters as a function of the overcooling rate. From the analysis of MD simulations, we extrapolate the thermodynamic properties for the clusters of arbitrary size up to the bulk.

The focus of our research is placed on the elucidation of correlated dynamics of a large ensemble of particles in the course of the nanoscale liquid-solid phase transition. Obviously, this problem is of significant interest and importance because the controlled dynamics of systems on the nanoscale is one of the central topics in the development of modern nanotechnologies. For the purposes of this analysis, we have chosen the melting process of Ni_{2057} clusters and performed a systematic theoretical analysis of its dynamics in the course of melting and solidification.

The choice of Ni clusters for these studies is motivated by their high chemical and catalytic reactivity, unique properties, and multiple applications in nanostructured materials.[34] An important example of such an application is the process of the catalytically activated growth of carbon nanotubes. The thermodynamic state of the catalytic nanoparticle plays a crucial role in the carbon nanotube growth.[35] The important question is whether the catalytic nanoparticle is molten or frozen during the nanotube growth process. It was demonstrated that when carbon nanotubes are grown on large 3–4 nm iron nanoparticles at temperatures lower than 1200 K, the catalytic particle is not completely molten.[24] Thus, the mechanism of nanotube growth can be governed by the surface melting of the cluster. Therefore, the advanced MD simulations of melting of large Ni clusters are important for a reliable evaluation of the conditions at which the carbon nanotube growth process takes place.[23,24,36,37] In order to achieve this task, it is necessary to perform MD simulations for relatively large nanoparticle sizes and large simulation times, which impose the use of the most advanced computational techniques based on the graphics processing units (GPUs). The advantages of this technology for MD simulations in comparison with the CPU-based one are demonstrated and benchmarked. The reported speedup reaches factors greater than 400.

The CPU calculations of the nickel clusters were carried out using a multipurpose computer code MESOBIONANO EXPLORER (MBN EXPLORER).[38] MBN EXPLORER allows us to use a broad variety of interatomic potentials to model different molecular systems, such as atomic clusters, fullerenes, nanotubes, polypeptides, proteins, DNA, composite systems, nanofractals, etc. Despite the universality, the computational efficiency of MBN EXPLORER is comparable (and in some cases even higher) than the computational efficiency of other software packages.

For the purposes of this work, we have adopted some of the MD algorithms of MBN EXPLORER to run them on GPUs. In particular, we have rewritten the part of the code responsible for calculations of the Sutton-Chen potential and forces using open computing language (OpenCL). OpenCL is a framework for writing programs that execute across heterogeneous platforms consisting of CPUs, GPUs, and other processors. The details of the implementation are discussed in the following section.

The paper is organized as follows. In Sec. II, we introduce the Sutton-Chen potential, describe the theoretical model of nucleation and growth of solid-state precursors in the course of the solidification phase transition, and present the details of the computational approach utilized in the work. In Sec. III, we demonstrate the results of MD simulations of Ni_{2047} clusters and analyze radial distribution function, diffusion coefficients for molten and solid states of the cluster, and the correspondence of MD simulation results with the theoretical model for the solidification rate. In Sec. IV, we draw conclusions to the paper.

II. THEORETICAL AND COMPUTATIONAL METHODS

A. Interaction potential for nickel atoms

The study of structural and dynamical properties of transition-metal clusters is a challenging task due to the presence of unfilled valence *d* orbitals. The high density of the *d* states and their delocalized character make the direct *ab initio* methods computationally very demanding for clusters larger than several tens of atoms.[39] In order to describe the structure of clusters of larger sizes, one needs to use approximate methods and model interatomic potentials.

An effective approach for the study of transition-metal clusters is the embedded-atom method,[40–45] which takes into account many-body effects. The latter appears through the inhomogeneous electron density of the system. In this paper, a MD study of nickel clusters has been performed using the Sutton-Chen[44] many-body potential, which belongs to the family of the embedded-atom types of potentials. The Sutton-Chen potential[44] has been shown to reproduce bulk and surface properties of transition metals and their alloys with sufficient accuracy (see, e.g., Refs. 39,46–49, and references therein). The applicability of the Sutton-Chen potential[44] to

Ni clusters has been proven by the direct comparison of the optimized structures and the binding energies of small Ni clusters obtained within the *ab initio* method and with the use of the Sutton-Chen potential.[39]

The potential energy of the finite system within the Sutton-Chen model has the following form:

$$U_{\text{pot}} = \varepsilon \sum_i \left[\frac{1}{2} \sum_{j \neq i} \left(\frac{a}{r_{ij}} \right)^n - c\rho_i^{1/2} \right], \tag{1}$$

where

$$\rho_i = \sum_{j \neq i} \left(\frac{a}{r_{ij}} \right)^m. \tag{2}$$

Here, r_{ij} is the distance between atoms i and j, ε is a parameter with dimension of energy, a is the lattice constant, c is a dimensionless parameter, and n and m are positive integers with $n > m$. The parameters provided by Sutton and Chen for nickel have the following values[44]: $\varepsilon = 1.5707 \times 10^{-2}$ eV, $a = 3.52$ Å, $c = 39.432$, $n = 9$, and $m = 6$. The parameters are fitted to the experimental values for bulk nickel in order to reproduce cohesive energy per atom, lattice parameter, and elastic constants. It should be mentioned that fitting of the parameters of the potential is done without any information on the thermal properties of nickel or on its liquid phase.

B. Theoretical model of the solidification kinetics

In the liquid-solid phase transition, the process of the formation of the new crystal phase in bulk is initiated by the formation of the stable precursor of the solid state. The energy of the formation of the precursor $E_p(r)$ of radius r can be written as follows:[50]

$$E_p(r) = \frac{4\pi r^2}{3} (3\alpha - r\Delta f), \tag{3}$$

where α is the liquid-solid surface tension coefficient and Δf is the difference of the free-energy densities for the liquid and the solid states. Here, we consider the process of crystallization from the overcooled liquid phase, therefore, Δf is positive and can be evaluated as follows:

$$\Delta f = f_l - f_s, \tag{4}$$

where f_l and f_s are the free-energy densities for the liquid and solid phases, correspondingly. f_l and f_s can be written as

$$f_l = e_{l0} + \frac{3NkT}{V_{cl}} - Ts_l, \tag{5}$$

$$f_s = e_{s0} + \frac{3NkT}{V_{cl}} - Ts_s, \tag{6}$$

where e_{l0}, e_{s0}, s_l, s_s, N, and V_{cl} are the ground-state energy densities of the liquid and solid phases, entropy densities of the liquid and solid states, number of atoms in the cluster, and cluster volume, correspondingly. The factor $3kT$ accounts for the energy stored in the thermal vibrations of the atoms at finite temperature. Using Eqs. (5) and (6), Eq. (4) can be written as follows:

$$\Delta f = \Delta s(T - T_0), \tag{7}$$

where $\Delta s = s_s - s_l$ and T_0 is the bulk phase transition temperature. For the derivation of Eq. (7) we have accounted for the fact that free-energy densities for both phases are equal at the bulk phase transition temperature, i.e., $e_{s0} - T_0 s_s = e_{l0} - T_0 s_l$.

Equation (3) has a maximum at certain values of r, corresponding to the critical size r_c of the precursor of the solid phase. If the size of the precursor is larger than r_c, its further growth will reduce the free energy of the system, and the crystal phase will expand. The value of r_c corresponds to the size at which the derivative over r of the Eq. (3) is equal to zero, i.e.,

$$r_c = \frac{2\alpha}{\Delta f}. \tag{8}$$

Substituting r_c from Eq. (8) into (3), one obtains the following value of the energy associated with the formation of the precursor of critical size:

$$E_p(r_c) = \frac{16\pi\alpha^3}{3\Delta s^2 (T - T_0)^2}, \tag{9}$$

where we have used Eq. (7) to substitute the expression for Δf.

Note that the precursors of the crystal phase are very improbable to be formed in the vicinity of the cluster surface since the surface atoms are in a liquidlike state even at the temperatures when the core of the cluster is in the solid state. The rate of the formation of the precursors of the solid phase can be calculated as follows:

$$k = A \exp\left[-\frac{16\pi\alpha^3}{3k_B T \Delta s^2 (T - T_0)^2} \right], \tag{10}$$

where k_B is the Boltzmann constant and A is the precursor formation frequency.

C. Computational approach

The numerical solution of the MD equations becomes a challenging task if one studies systems with a large number of atoms. Generally, the crucial time-consuming part of the computation is the calculation of the forces between the particles at each time step. For two-body forces, this implies a computational effort rising with N^2, where N is the number of atoms (see Fig. 1). An implicit many-body structure of the force as it is generated by the second term in the Sutton-Chen potential [Eq. (1)] can potentially increase the calculation effort.

As the force calculation essentially implies the same type of calculation repeated many times over, this task is ideally suited to be implemented using a parallel-programming approach. If there are only few different types of forces involved, as is the case discussed here, a single-instruction multiple-data (SIMD) hardware environment can be adopted in a natural way since the same instructions are used for all pairs of particles. Graphics cards (GPUs) fulfill these requirements in an ideal way. We therefore ported our original CPU-based code MBN EXPLORER (Ref. 38) for CUDA as well as OpenCL programming frameworks. We reduced the many-body part of the calculation to two successive two-body problems, in the

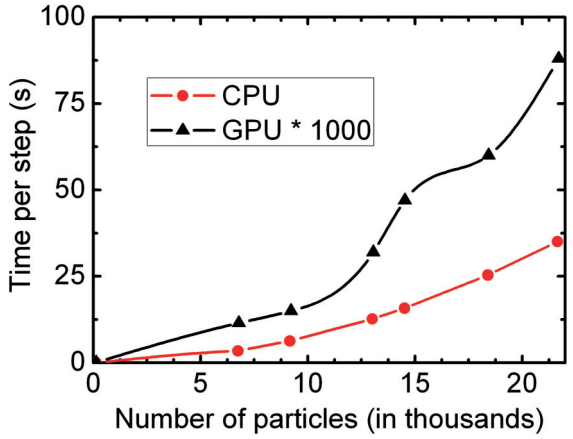

FIG. 1. (Color online) Dependence of computation time on the system size. From the figure it is seen that the time is proportional to the squared number of particles, i.e., $\mathcal{O}(N^2)$. Note that the time per step is multiplied by 1000 for the GPU case.

first sweep calculating all ρ_i in Eq. (2) and then determining the forces on the atoms.

The calculations presented here were performed on the LOEWE computer cluster at Frankfurt University, which features 778 graphics cards Radeon HD 5870. Each card includes 1600 streaming processors clocked at 850 MHz. The resulting GPU calculations were compared to a single core of Intel Core i7 870 CPU.

Figure 2 shows the speedup of a MD simulation of nickel clusters of different sizes comparing CPU and GPU versions of the code. As can be seen, one can achieve speedups of more than two orders of magnitude for larger clusters. According to AMD Radeon specifications, the GPU card has 2720 GFLOPS in single precision and one core of Core i7 CPU can be estimated as having nearly 15 GFLOPS in double precision. This theoretical speedup factor of nearly 200 (with additional exploitation of very fast local memory and specific mathematical functions on the GPU) shows that in comparison with our measured speedup factor, the OpenCL implementation makes full use of the advantages of the GPU environment. In double precision, the difference would be less as AMD Radeon is specified to have 544 GFLOPS in double

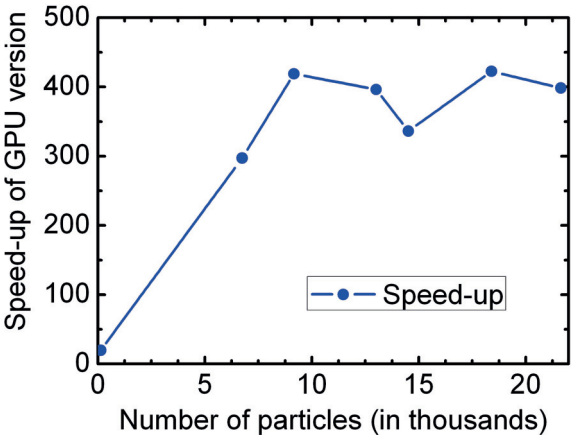

FIG. 2. (Color online) Speedup of the computational time for GPU as compared to the CPU version.

precession. It means that for a double precision code, one can expect speedup of nearly 100 over the single threaded code.

In our code, each particle was assigned to a certain thread. It implies that if the number of particles is smaller than the number of stream processors, GPUs will not be completely loaded. In order to utilize the GPUs efficiently, the number of particles should be an integer multiple of the number of the stream processors. This can be seen on speedup plots presented in Figs. 1 and 2. Speedup growth is nearly linear until 10 000 particles. For the number of particles exceeding 10 000, the speedup saturates to a constant level, corresponding to full utilization of the GPU. In the presented benchmarks, the GPU computation time was averaged over 1000 iterations in order to avoid accounting for random slowdowns and lags. CPU computation time was averaged over 10 iterations since random slowdowns of CPU are expected to have minor influence on the computational time.

Current calculations were performed as full N-body calculation without spatial cutoff for the interaction of the atoms, i.e., taking into account interactions between all atoms of the cluster. Therefore, in this work we have studied the cluster consisting of ∼2000 atoms, where a cutoff does not have a substantial advantage in computing time, but the speedup due to utilization of GPUs is about 100. The number of atoms in the cluster was chosen as an optimal balance between the maximal size of the system and longest achievable simulation time scales. Long simulation time is necessary to probe the solidification kinetics at temperatures close to the phase transition. The efficient implementation of interaction cutoffs in the GPU code is in progress and will be adopted and discussed in forthcoming work. The MD simulations were carried out using a Verlet integrator with a time step of 1 fs. The temperature control was carried out using a Langevin thermostat with a damping constant of 10 ps^{-1}.

III. RESULTS AND DISCUSSION

A. MD simulations of Ni_{2047} clusters

We have performed MD simulations of Ni_{2047} clusters. The initial geometry of the cluster was chosen to resemble icosahedral symmetry. Then, the particle was exposed to the heating-cooling cycle with the heating/cooling rate of 1 K/ps in the temperature range from 400 to 1400 K. From Fig. 3 is is seen that the final structure of the crystallized particle (blue dots at low temperatures) has lower energy than the initial icosahedral structure. The method to obtain molecular structures with higher binding energy by exposing the heated system to the cooling temperature bath is a widely used technique in MD simulations and is known as simulated annealing.[51] The lowering of the nickel cluster's energy after the resolidification form icosahedral structure happens due to the formation of regions with fcc symmetry in the relatively large nickel clusters.[30] From Fig. 3 is also seen a prominent hysteresis in the melting and crystallization phase transitions due to the finite speed of the heating and cooling rates. Note that the width of the hysteresis is almost 400 K for the heating/cooling rate of 1 K/ps, which shows that the crystallization process in the system is associated with transfer over a relatively high free-energy barrier. In the following

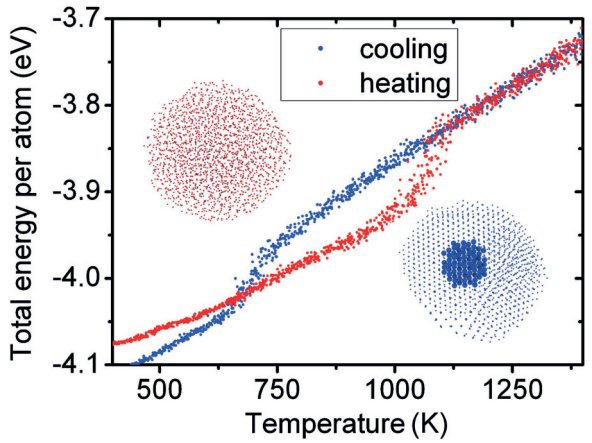

FIG. 3. (Color online) Dependence of the total energy per atom in heating (red) and cooling (blue) simulations. In the insets are shown the structures of Ni_{2047} in the molten (top left) and solidified (bottom right) states. The fragment of crystal structure is shown by blue spheres inside the crystallized structure.

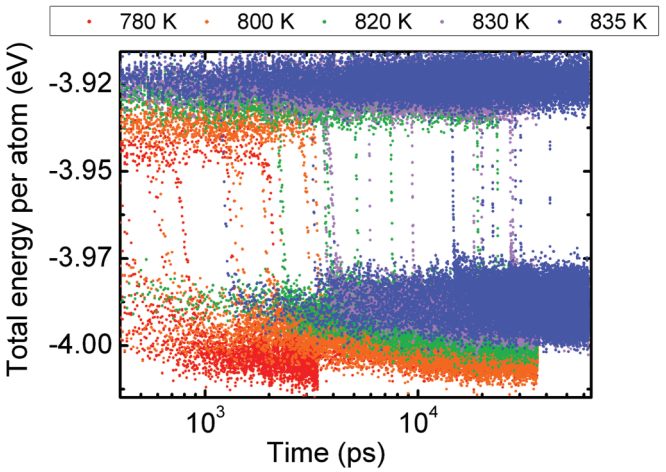

FIG. 4. (Color online) Dependencies on time of the total energy per atom for the cluster being initially in the molten state at different temperatures of the thermostat. Red, orange, green, magenta, and violet dots correspond to thermostat temperature of 780, 800, 820, 830, and 835 K, correspondingly. Note the logarithm scale on the horizontal time axis. The solidification phase transition occurs earlier in the systems with lower temperature.

section, we investigate the dynamics of the crystallization transition.

B. Solidification process in Ni_{2047} clusters

By means of MD simulations, we have investigated the solidification kinetics of the Ni_{2047} cluster as a function of the amount of overcooling. The initial structure of the cluster was taken from MD simulations above the melting temperature. Then, the initially molten cluster was simulated at various temperatures below the melting point. We have investigated the time needed for the system to change its phase from the molten to the solid state as a function of the temperature below the phase transition point. The simulations were performed at 780, 800, 820, 830, and 835 K. For each temperature, up to 15 independent simulations were produced. Figure 4 shows the dependence of the total energy of the system on the simulation time for five randomly chosen trajectories for each value of temperature in the range between 740 and 820 K. Note the logarithm scale on the horizontal axes.

From Fig. 4, it is seen that at certain moments of time the energy of the system abruptly changes. These moments correspond to the transition of the system from the molten to the solid state. Indeed, the solid state of the cluster corresponds to the increased binding energy between the atoms due to the formation of the regular crystal lattice, which leads to the lowering of the total energy of the system.

C. Radial distribution function as an indicator of the phase transition

In this section, we analyze to which extent the radial distribution function (RDF) for atoms in the cluster becomes affected by the solidification phase transition. The RDF $g(r)$ is defined as

$$g(r) = \frac{N(r,\delta r)}{4\pi r^2 \delta r}\frac{1}{\bar{\rho}}, \tag{11}$$

where $N(r,\delta r)$ is the number of atoms located in the spherical shell of width δr and radius r forms a reference particle and $\bar{\rho}$ is an average density of the particles in the system. $g(r)$ characterizes the number of particles at the certain radial distance from a reference particle.

We have calculated the RDF for nickel clusters in solid and molten states. The following procedure was adopted for the calculation of the RDF. At certain instances of time, the atoms located within 4 Å of the cluster center of mass were selected. For these atoms, the RDF was calculated with a distance bin of 0.14 Å and averaged over 1 consequent nanosecond of simulation, which results in averaging over 100 cluster structures since we have written the structure of the system each with 10 ps of simulation. The RDF for the central atoms was calculated as an average over RDFs for atoms of each of 100 structures. The average density $\bar{\rho}$ was calculated as the ratio of the number of atoms located within 4 Å from the cluster center and the volume of a sphere with radius 4 Å.

We analyzed one particular trajectory of the MD simulations at the thermostat temperature equal to 820 K (see orange trajectories in Fig. 4). For the chosen trajectory, the solidification transition occurs 7.4 ns after the start of the simulation. The RDF for that trajectory at various instances of time is plotted using B-splines in Fig. 5.

From Fig. 5 it is seen that RDFs at 0, 5, and 7 ns (red, orange, and green curves) are substantially different form those plotted for later time instances. This, obviously, can be explained by the formation of cluster crystalline structure upon solidification. Indeed, peaks at ~4.5 and ~6.5 Å are more pronounced for the RDFs at 8–9 ns since the crystalline structure has a long-range order. Note that the RDF at 7 ns attains some features of RDFs characteristic for the crystallized state, however, the crystallization transition takes place at 7.4 ns. This is related to the fact the calculated RDF was averaged over 1 ns in order to increase the statistics. Therefore, the RDF at 7 ns was partially constructed from the cluster structures being in crystalline state.

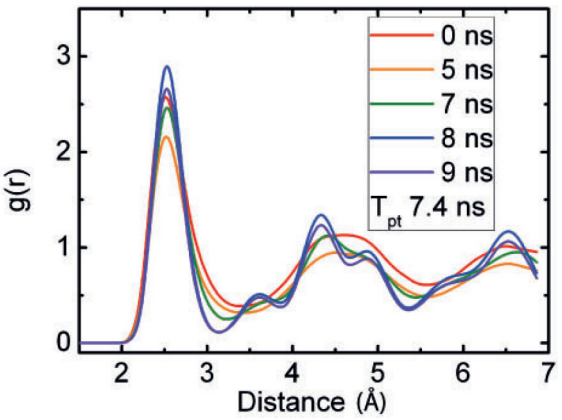

FIG. 5. (Color online) Radial distribution function for the most central atoms of the Ni_{2047} cluster at different instances of simulation time. For the selected analysis trajectory, the solidification transition had occurred at $T_{pt} = 7.4$ ns.

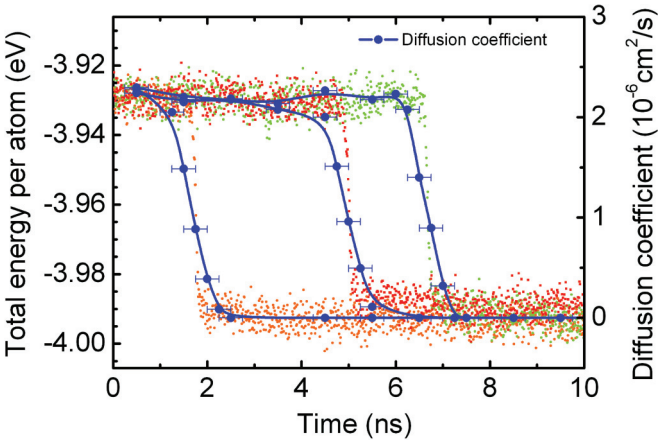

FIG. 6. (Color online) Left axis: dependencies of the total energy per atom on time. Colors indicate different MD trajectories. Right axis: dependence of diffusion coefficient on time.

Despite that RDF can be used for the characterization of the melting-solidification transition in the system, it is not entirely clear as to how to define uniquely the phase transition moment from the RDF analysis, especially when RDFs are calculated with a reduced amount of sampling data, which is often the case for finite systems. In the next section, we report on the analysis of the diffusion coefficient behavior which turns out to be a much more convenient quantity for the characterization of the liquid-solid phase transition.

D. Diffusion coefficient as a fingerprint of solidification phase transition

The diffusion coefficient of a particle is defined as follows:

$$D = \frac{\langle \Delta r^2 \rangle}{2z\Delta t}, \tag{12}$$

where $\langle \Delta r^2 \rangle$ is a mean-square displacement of a particle per time Δt, and z is dimensionality of space (3 for three-dimensional diffusion).[52]

The variation of diffusion coefficient at solid-liquid phase transition in MD simulations of Ar_{13} clusters was discussed more than two decades ago in the work by Jellinek and co-workers.[53] In Ref. 28, the diffusion coefficient for Na_{142} clusters was calculated for the temperatures below and above the melting point.

We have calculated the self-diffusion coefficient of nickel atoms located in the central part of the cluster at different instances of time. For the analysis, we have chosen three out five MD trajectories of the N_{2057} cluster conducted with a thermostat temperature equal to 820 K. The total energy of the system and the diffusion coefficient as functions of time are plotted for each trajectory in Fig. 6.

The following procedure was used for the calculation of the self-diffusion coefficient: the part of the MD trajectory starting 0.5 ns before and ending 0.5 ns after each given instant of time was selected and the coordinates of all atoms were recorded. For each structure, the cluster was translated and rotated as a whole in order to minimize the root-mean-square displacement of atoms from a reference structure. This procedure allows us to exclude rotational and translational motion of the cluster when calculating the diffusion coefficient. Then, the selected part of the trajectory was split into 10 segments and the diffusion coefficient was calculated for all atoms located within 10 Å of the cluster center of mass using Eq. (12). The final value of the diffusion coefficient was calculated as an average over all central atoms and 10 trajectory segments. Since the diffusion coefficient was calculated as an average over 1 ns of the MD simulation, in Fig. 6 we show the corresponding horizontal error bars for each value of the diffusion coefficient.

From Fig. 6 it is seen that for all three trajectories, the diffusion coefficient drops abruptly at certain moments of time exactly corresponding to the moment of the solidification phase transition. The value of the diffusion coefficient for the molten state is $\sim 2.3 \times 10^{-6}$ cm^2/s. These values are in good correspondence to those reported in Ref. 30.

The analysis of root-mean-square displacement (RMSD) of atoms in Ni_{1004} clusters at various temperature was reported in Ref. 30. In that work, MD simulations were performed using the quantum-corrected Sutton-Chen potential.[54] The RMSD of nickel atoms in the core shells of the cluster was calculated to be 1.0–1.2 Å at the temperatures above the phase transition. The RMSD was calculated after 10 ps of MD simulations, which correspond to the diffusion coefficient of $1.7–3.3 \times 10^{-6}$ cm^2/s depending on the distance of atoms form the cluster center. In Ref. 55, the nickel atoms were modeled with periodic boundary conditions using many-body potential due to Cleri and Rosato.[56] In that work, the diffusion coefficient of the nickel atoms was reported to be 3.7×10^{-5} cm^2/s at 1728 K. In Ref. 57, the diffusion coefficient for nickel atoms simulated with periodic boundary conditions was calculated to be 2.52×10^{-5} cm^2/s at 1785 K. The discrepancies between our results and the aforementioned works can be attributed to utilization of different potentials for interatomic interactions, and to the fact that we calculate the diffusion coefficient at much lower temperature, as compared to Refs. 55 and 57.

The diffusion coefficient in the solid state appears to be smaller than 10^{-6}–10^{-7} cm^2/s. We were not able to evaluate it accurately for a given set of data since it requires more than 5 ns to observe even a single event of exchange of mutual positions for a pair of atoms at 820 K. From Fig. 6 it is seen that the dependence of the diffusion coefficient on time qualitatively

reproduces well the time dependence of the total energy. One can use the diffusion coefficient as a reliable indicator of the phase transition.

E. Kinetics of the solidification phase transition

In this section, we evaluate thermodynamic characteristics of the solidification phase transition on the basis of the analysis of kinetics of this process obtained from MD simulations. We calculate the latent heat of the phase transition as a difference of the averaged total energy of the system in molten and solid states. For the Ni_{2047} cluster, the latent heat of the phase transition ΔE is equal to 127.8 eV. The entropy density change between solid and molten states of the cluster can be calculated as follows:

$$\Delta s = \frac{\Delta E}{T_0 V_{cl}}, \tag{13}$$

where T_0 and V_{cl} are a phase transition temperature and a cluster volume, correspondingly. Note that here we neglect the fact that the surface layer of the atoms of the cluster remains liquid after the solidification of the cluster core.

In Table I, we present the lifetime of the system in an overcooled state for a temperature range between 780 and 835 K. The time of the phase transition was defined as a moment at which the energy of the system starts to decrease rapidly due to the formation of the solid phase. The last row in Table I shows the escape rate from the overcooled states, which is defined as

$$\kappa = (\langle t \rangle)^{-1}, \tag{14}$$

where $\langle t \rangle$ denotes averaging of the lifetime over the simulation runs for the corresponding temperature.

The fraction of clusters in the liquid state below the phase transition temperature as a function of time $c(t)$ can be approximated with the following expression:

$$c(t) = \exp(-\kappa t), \tag{15}$$

where κ can be evaluated using Eq. (14). In Fig. 7, the results of the MD simulations are shown by dots. Solid lines correspond to the exponential reduction of the fraction of liquid clusters as derived using Eq. (15).

Values of κ obtained from the MD simulations are shown in Fig. 8 by blue dots. The error bars correspond to the single standard deviation calculated for a set of data for each temperature value. According to the theoretical model presented in Sec. II, the solidification rate can be described using Eq. (10). We can take the logarithm from both sides of Eq. (10) and rewrite it as follows:

$$\ln(\kappa 1 f s) = a - \frac{b}{k_B T (T - T_0)^2}, \tag{16}$$

where $a = \ln A$ and $b = 16\pi\alpha^3/(3\Delta s^2)$. We treat a, b, and T_0 as free parameters and perform the least-squares numerical

TABLE I. Lifetime in picoseconds of the overcooled liquid state for different MD trajectories at various temperatures. 15 simulations were performed for 780 and 800 K, 12 for 820 K, and 10 simulations for 830 and 835 K.

	780 K	800 K	820 K	830 K	835 K
1	80	110	100	3610	1160
2	170	170	1740	3730	3320
3	230	180	2260	9340	5890
4	240	550	3600	18130	14680
5	280	820	5020	19080	20008
6	310	890	5130	19760	22240
7	360	1260	6670	22640	28640
8	370	1320	7430	26670	30230
9	380	1390	7800	27670	41670
10	530	1600	9450	36380	63180
11	540	1830	11620		
12	570	1930	23400		
13	740	2210			
14	750	2800			
15	2000	3610			
Mean (ps)	503	1378	6440	18731	23102
κ (10^{-5} ps^{-1})	199	72.6	15.5	5.34	4.33

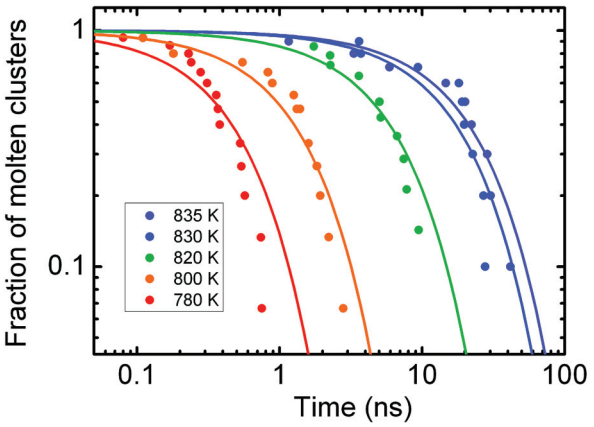

FIG. 7. (Color online) Fraction of Ni_{2057} clusters in the molten state as a function of simulation time for various temperatures below the phase transition point. Dots show the results obtained from MD simulations. Numerical fit of the results using Eq. (10) is shown by solid lines.

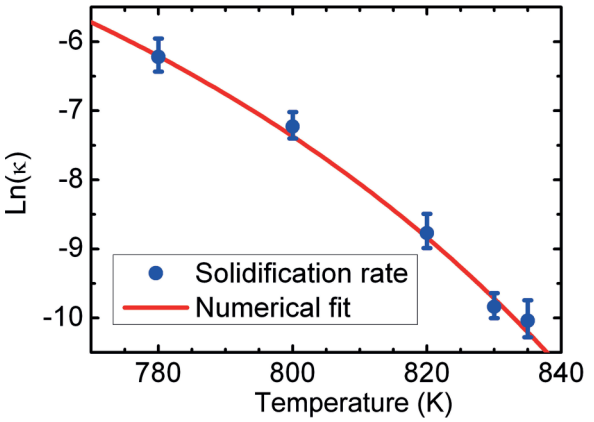

FIG. 8. (Color online) Solidification rate of Ni_{2057} cluster for various temperatures below the phase transition point. Error bars correspond to a single standard deviation calculated for a set of data for each temperature value. Numerical least-squares fit of the results using Eq. (16) is shown by a solid line.

fitting of the rates obtained form MD simulations at various temperatures. The result of this fitting is shown by a solid line in Fig. 8. From the fitting, we have obtained the following values of the parameters: $a = 1.24$, $b = 31\,053$ eV K^2, and $T_0 = 1029$ K. Therefore, according to the theoretical model, the precursor formation frequency [coefficient A in Eq. (10)] is 3.5 ps^{-1} and the phase transition temperature of the bulk nickel material for the used parametrization of the Sutton-Chen potential (T_0) is equal to 1029 K.

Note that the value of T_0 is obtained within the framework suggested in the theoretical model of Sec. II, which is based on a number of assumptions. The theoretical model does not account for the effects associated with the change of crystal symmetry in the precursors of various sizes, does not account for geometrical shell closure effects, neglects presence of cluster-vacuum boundary in the system, and assumes spherical geometry of the precursor. Accounting for the aforementioned effect may influence the value T_0. However, we do not expect that such influence should be very significant and we leave the problem of more accurate derivation of T_0 for further consideration.

This value of the phase transition temperature is lower than that reported in Ref. 32, where the phase transition of bulk nickel for the similar parametrization of the Sutton-Chen potential was calculated to be 1160 K. The discrepancies between our results and the results of previous calculations are largely because of utilization of a cutoff of 7.08 Å in Ref. 32 and limited statistics for the calculation of the overcooled cluster lifetimes in this work.

Evaluating Δs using Eq. (13), one can calculate the liquid-solid surface tension coefficient α as a real root of the following equation:

$$\frac{16\pi\alpha^3}{3\Delta s^2} = b. \tag{17}$$

Solving Eq. (17), one obtains $\alpha = 0.53$ eV/nm^2 or 85 mJ/m^2. This value of α is approximately two times lower than that reported in Ref. 30 for the nickel crystal-liquid tension coefficient. The discrepancy can be attributed to the various parametrizations of the Sutton-Chen potential used in our and their works.

Knowing the surface tension coefficient α, one can calculate the critical size of the precursor of the solid phase for different temperatures using Eqs. (8) and (13). From those equations, it follows that the critical precursor consists of 26, 33, 41, 53, 70, 80, and 87 atoms for the temperature equal to 740, 760, 780, 800, 820, 830, and 835 K, correspondingly.

From Eq. (8) it is seen that the critical size of the precursor grows when the temperature of the system approaches the phase transition temperature of the bulk. However, for finite systems the size of the critical precursor can not be larger than the cluster size. We can use this idea to calculate the phase transition temperature of the finite-size cluster systems as follows:

$$T(N) = T_0 - \left(\frac{4\pi\rho}{3N}\right)^{1/3} \frac{2\alpha}{\Delta s}, \tag{18}$$

where N denotes the number of particles in the cluster and ρ is the particle density. This equation is also known as the Gibbs-Thomson equation describing the suppression of the melting point of the solid particles in their own fluid. From Eq. (18) it follows that the suppression of the melting point is inversely proportional to the number of atoms in the cluster in the power of one third, and the melting point of the cluster consisting of 2057 atoms is equal to 962 K.

IV. CONCLUSIONS

In this paper, we have conducted classical MD simulations of the Ni_{2047} cluster with the use of the many-body Sutton-Chen potential on time scales up to 65 ns. For the purposes of this work, we have developed an efficient software code capable of performing large-scale MD simulations on GPUs. We have demonstrated that with the use of GPU technology, one can achieve the speedup of computations up to 400 times as compared to single-core CPU. On the basis of MD simulations, we have investigated the radial distribution function and the diffusion coefficient at molten and solidified states of the system. We have shown the applicability of RDF and diffusion coefficients as markers of the phase transition. We have analyzed the solidification kinetics of the clusters as a function of the overcooling temperature and shown that the kinetics of the phase transition in Ni_{2057} clusters can be described within the framework of the precursor formation theoretical model. Based on that theoretical model, we had derived various characteristics of the systems such as solid-liquid surface tension coefficient, rate of the precursors formation,and the phase transition temperature for the clusters of arbitrary size. Utilization of GPU has allowed us to investigate the solidification kinetics on long time scales close to the phase transition temperature. Analysis of the solidification rates has confirmed the validity of the solid-state precursor formation mechanism in the nickel clusters with the radius of 1.5 nm, which is the major result of this work. We demonstrate a recipe to evaluate various thermodynamic characteristics of the finite system from a single set of MD simulations data. Further work can be devoted to the optimization of the GPU code, and the investigation of the solidification kinetics of clusters of various sizes or of different atoms, and clusters consisting of mixture of different metals (nanoalloys). With extension of the GPU code, one can perform MD simulations of the solid-liquid phase transition with periodic boundary conditions and derive the melting temperature for the bulk material, which can be compared to the value of the bulk phase transition temperature T_0 obtained using the suggested theoretical model. One can also investigate the influence of impurities on the solidification kinetics. Another direction of the research can be devoted to the analysis of various criteria characterizing the phase transition, such as the Lindemann criterion, two- or three-particle correlation functions, etc.

ACKNOWLEDGMENTS

The authors acknowledge the Frankfurt Center for Scientific Computing for the possibility to perform complex computer simulation using CPU and GPU. A.V.Y. thanks Stiftung Polytechnische Gesellschaft Frankfurt am Main for financial support.

*On leave from A.F. Ioffe Physical-Technical Institute, Politechnicheskaya 26, 194021 St. Petersburg, Russia.
[1]A. Aguado and M. Jarrold, Annu. Rev. Phys. Chem. **62**, 151 (2011).
[2]D. Turnbull, J. Appl. Physiol. **21**, 1022 (1950).
[3]D. Turnbull, J. Chem. Phys. **20**, 411 (1952).
[4]P. Pawlow, Z. Physik. Chem. **65**, 545 (1909).
[5]P. Buffat and J.-P. Borel, Phys. Rev. A **13**, 2287 (1976).
[6]T. Castro, R. Reifenberger, E. Choi, and R. P. Andres, Phys. Rev. B **42**, 8548 (1990).
[7]S. L. Lai, J. Y. Guo, V. Petrova, G. Ramanath, and L. H. Allen, Phys. Rev. Lett. **77**, 99 (1996).
[8]C. E. Bottani, A. Li Bassi, B. K. Tanner, A. Stella, P. Tognini, P. Cheyssac, and R. Kofman, Phys. Rev. B **59**, R15601 (1999).
[9]M. Schmidt, R. Kusche, W. Kronmüller, B. von Issendorff, and H. Haberland, Phys. Rev. Lett. **79**, 99 (1997).
[10]M. Schmidt, R. Kusche, B. von Issendorff, and H. Haberland, Nature (London) **393**, 238 (1998).
[11]R. Kusche, Th. Hippler, M. Schmidt, B. von Issendorff, and H. Haberland, Eur. Phys. J. D **9**, 1 (1999).
[12]H. Haberland, T. Hippler, J. Donges, O. Kostko, M. Schmidt, and B. von Issendorff, Phys. Rev. Lett. **94**, 035701 (2005).
[13]F. Calvo and F. Spiegelmann, J. Chem. Phys. **112**, 2888 (2006).
[14]J. A. Reyes-Nava, I. L. Garzon, and K. Michaelian, Phys. Rev. B **67**, 165401 (2003).
[15]F. Calvo and F. Spiegelmann, J. Chem. Phys. **120**, 9684 (2004).
[16]K. Manninen, A. Rytkonen, and M. Manninen, Eur. Phys. J. D **29**, 39 (2004).
[17]S. Chacko, D. G. Kanhere, and S. A. Blundell, Phys. Rev. B **71**, 155407 (2005).
[18]A. Aguado and J. M. López, Phys. Rev. Lett. **94**, 233401 (2005).
[19]A. Aguado, J. Phys. Chem. B **109**, 13043 (2005).
[20]E. Noya, J. Doye, D. Wales, and A. Aguado, Eur. Phys. J. D **43**, 57 (2007).
[21]A. A. Shvartsburg and M. F. Jarrold, Phys. Rev. Lett. **85**, 2530 (2000).
[22]G. A. Breaux, R. C. Benirschke, T. Sugai, B. S. Kinnear, and M. F. Jarrold, Phys. Rev. Lett. **91**, 215508 (2003).
[23]A. Lyalin, A. Hussien, A. V. Solov'yov, and W. Greiner, Phys. Rev. B **79**, 165403 (2009).
[24]F. Ding, K. Bolton, and A. Rosn, J. Vac. Sci. Technol. A **22**, 1471 (2004).
[25]A. Q. Jiang, N. Awasthi, A. N. Kolmogorov, W. Setyawan, A. Borjesson, K. Bolton, A. R. Harutyunyan, and S. Curtarolo, Phys. Rev. B **75**, 205426 (2007).
[26]O. Petrov and I. Furo, Phys. Rev. E **73**, 011608 (2006).
[27]A. V. Ruban and I. A. Abrikosov, Rep. Prog. Phys. **71**, 046501 (2008).
[28]A. Aguado, J. M. López, J. A. Alonso, and M. J. Stott, J. Phys. Chem. B **105**, 2386 (2001).
[29]C. M. Goringe, D. R. Bowler, and E. Hernández, Rep. Prog. Phys. **60**, 1447 (1999).
[30]Q. Yue, T. Cagin, W. Johnson, and W. Goddard, J. Chem. Phys. **115**, 385 (2001).
[31]Y. Qi, T. Çağın, Y. Kimura, and W. A. Goddard, Phys. Rev. B **59**, 3527 (1999).
[32]Y. Shibuta and T. Suzuki, Chem. Phys. Lett. **498**, 323 (2010).
[33]Y. Shibuta and T. Suzuki, Chem. Phys. Lett. **502**, 82 (2011).
[34]*Handbook of Nanoscience, Engineering, and Technology*, edited by W. Goddard, D. Brenner, S. Lyshevski, and G. Iafrate (CRC Press, Boca Raton, FL, 2007).
[35]A. Harutyunyan, T. Tokune, and E. Mora, Appl. Phys. Lett. **87**, 051919 (2005).
[36]O. Obolensky, I. Solov'yov, A. Solov'yov, and W. Greiner, in *International Symposium ISACC 2007*, edited by A. Solov'yov (Imperial College Press, London, 2007), Vol. 31D, p. 176.
[37]A. R. Harutyunyan, N. Awasthi, A. Jiang, W. Setyawan, E. Mora, T. Tokune, K. Bolton, and S. Curtarolo, Phys. Rev. Lett. **100**, 195502 (2008).
[38]I. Solov'yov, A. Yakubovich, P. Nikolaev, I. Volkovets, and A. Solov'yov, J. Comp. Chem. **33**, 2412 (2012).
[39]S. Nayak, S. Khanna, B. Rao, and P. Jena, J. Phys. Chem. A **101**, 1072 (1997).
[40]M. Daw and M. Baskes, Phys. Rev. Lett. **50**, 1285 (1983).
[41]M. S. Daw and M. I. Baskes, Phys. Rev. B **29**, 6443 (1984).
[42]M. Finnis and J. Sinclair, Philos. Mag. **50**, 45 (1984).
[43]S. M. Foiles, M. I. Baskes, and M. S. Daw, Phys. Rev. B **33**, 7983 (1986).
[44]A. Sutton and J. Chen, Philos. Mag. Lett. **61**, 139 (1990).
[45]A. P. Sutton, P. D. Godwin, and A. P. Horsfield, MRS Bull. **21**, 42 (1996).
[46]H. Raffi-Tabar and A. Sutton, Philos. Mag. Lett. **63**, 217 (1991).
[47]B. Todd and R. Lynden-Bell, Surf. Sci. **287**, 191 (1993).
[48]R. Lynden-Bell, J. Phys.: Condens. Matter **7**, 4603 (1995).
[49]J. Doye and D. Wales, New J. Chem. **22**, 733 (1998).
[50]L. Landau and E. Lifshitz, *Statistical Physics, Part I* (Butterworth-Heinemann, Oxford, 1980).
[51]S. Kirkpatrick, C. Gelatt, and M. Vecchi, Science **220**, 671 (1983).
[52]V. V. Dick, I. A. Solov'yov, and A. V. Solov'yov, Phys. Rev. B **84**, 115408 (2011).
[53]J. Jellinek, T. L. Beck, and R. S. Berry, J. Chem. Phys. **84**, 2783 (1986).
[54]T. Cagin, Y. Qi, H. Li, Y. Kimura, H. Ikeda, W. Johnson, and W. Goddard III, MRS Symp. Ser. **554**, 43 (1999).
[55]O. N. Bedoya-Martínez, M. Kaczmarski, and E. R. Hernández, J. Phys.: Condens. Matter **18**, 8049 (2006).
[56]F. Cleri and V. Rosato, Phys. Rev. B **48**, 22 (1993).
[57]M. M. G. Alemany, O. Diéguez, C. Rey, and L. J. Gallego, Phys. Rev. B **60**, 9208 (1999).